Supporting Information (SI)

Electrochemical-reconstructed WC/WO_2-WO_3 heterostructure as a highly efficient hydrogen oxidation electrocatalyst

Ge Meng,[ab] Heliang Yao,[a] Han Tian,[a] Fantao Kong,[a] Xiangzhi Cui,*[abc] Shaowen Cao,[d] Yafeng Chen,[e] Ziwei Chang,[af] Chang Chen,[ab] Jianlin Shi,*[ab]

[a]State Key Laboratory of High Performance Ceramics and Superfine Microstructure, Shanghai Institute of Ceramics, Chinese Academy of Sciences, Shanghai, 200050, P.R. China.

[b]Center of Materials Science and Optoelectronics Engineering, University of Chinese Academy of Sciences, Beijing, 100049, P.R. China.

[c]School of Chemistry and Materials Science, Hangzhou Institute for Advanced Study, University of Chinese Academy of Sciences, Hangzhou 310024, P.R. China.

[d]State Key Laboratory of Advanced Technology for Materials Synthesis and Processing, Wuhan University of Technology, Wuhan, 430070, P.R. China.

[e]Beijing Advanced Innovation Center for Materials Genome Engineering, Collaborative Innovation Center of Steel Technology, University of Science and Technology Beijing, Beijing, 100083, P.R. China.

[f]School of Physical Science and Technology, Shanghai Tech University, Shanghai, 201210, P.R. China

*Email: cuixz@mail.sic.ac.cn, jlshi@mail.si.ac.cn

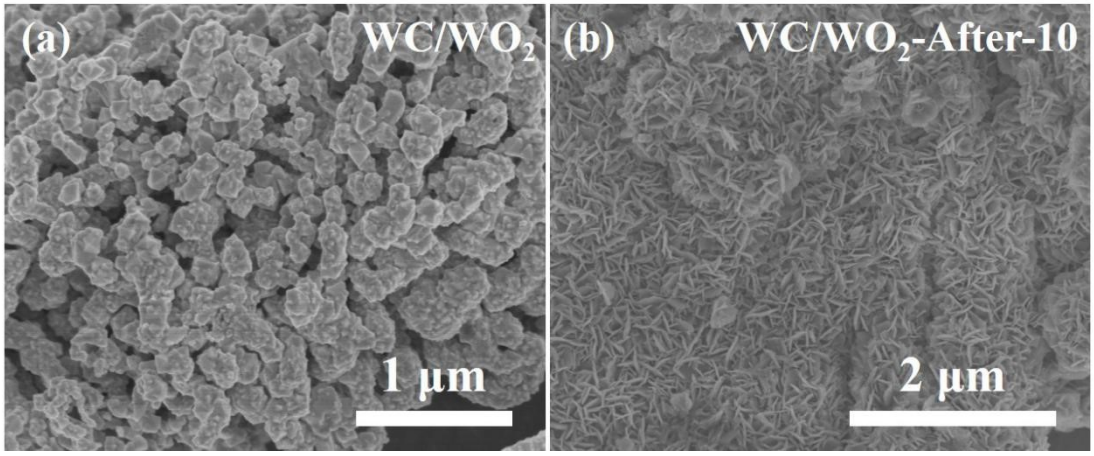

Figure S1. SEM images of pristine WC/WO_2 (a) and WC/WO_2-After-10 (b).

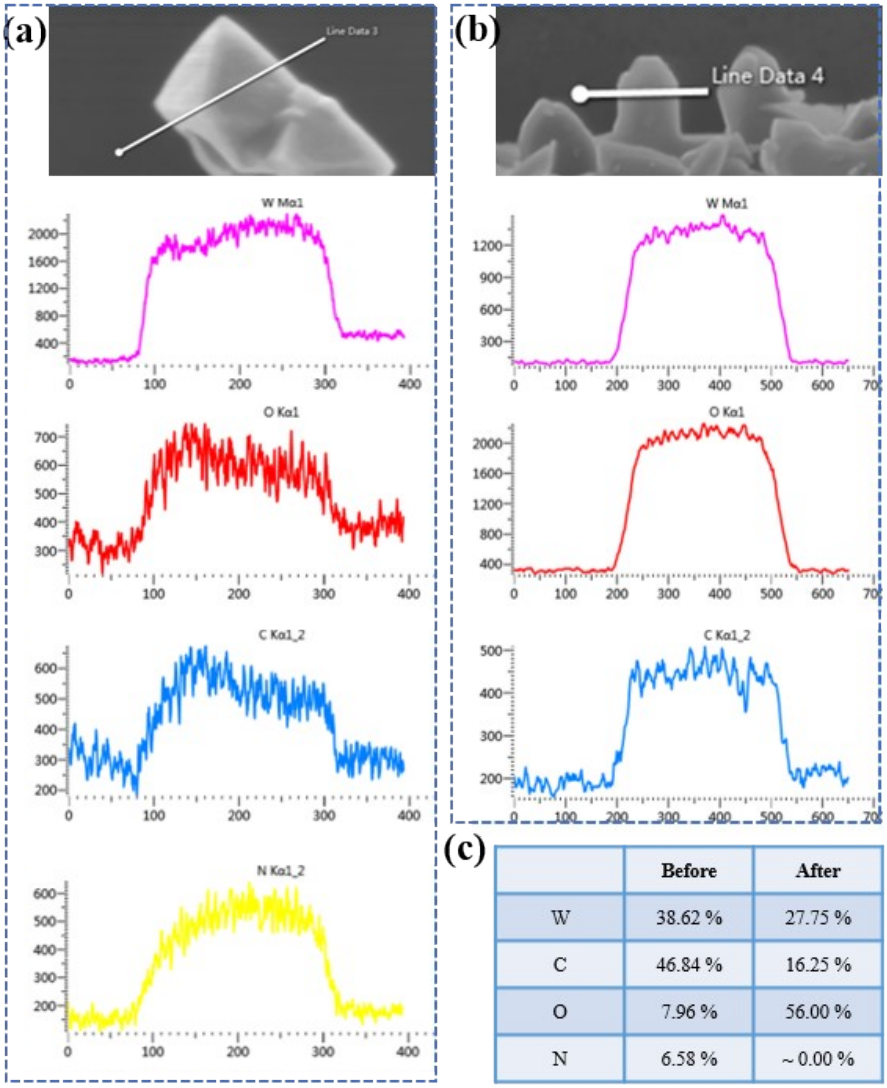

(c)

	Before	After
W	38.62 %	27.75 %
C	46.84 %	16.25 %
O	7.96 %	56.00 %
N	6.58 %	~ 0.00 %

Figure S2. Liner elemental scanning profiles of pristine WC/WO_2 (a) and WC/WO_2-After-10 (b). (c) Corresponding elemental concentrations (wt. %).

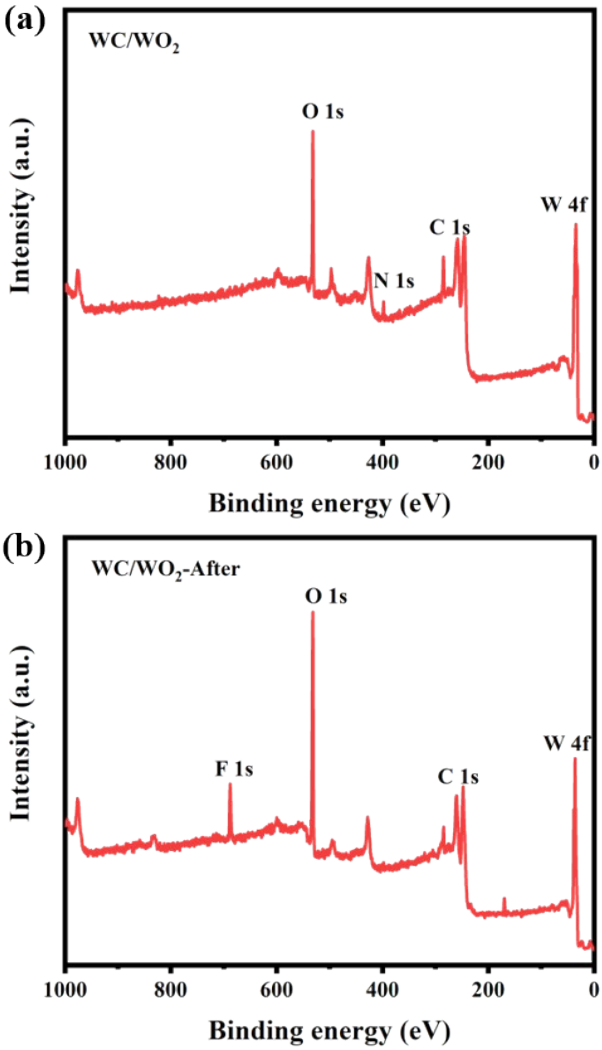

Figure S3. XPS survey spectra of WC/WO_2 (a) and WC/WO_2-After-10 (b).

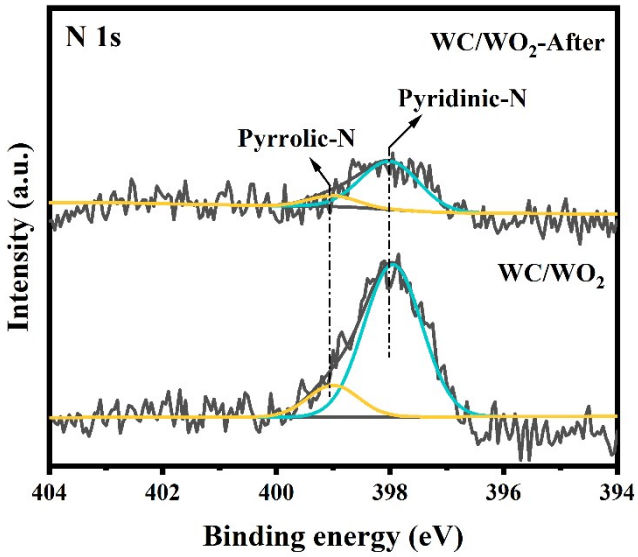

Figure S4. XPS N 1s spectra of WC/WO_2 and WC/WO_2-After-10.

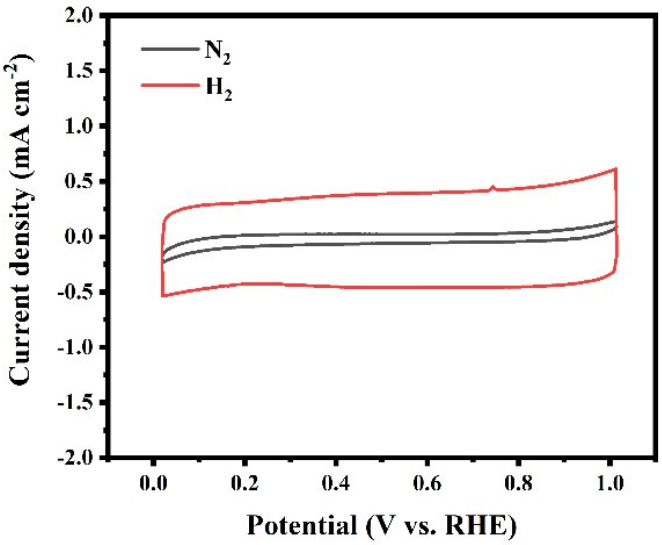

Figure S5. CV curves tested in N_2 or H_2 saturated 0.5 M H_2SO_4 of the pristine WC/WO_2.

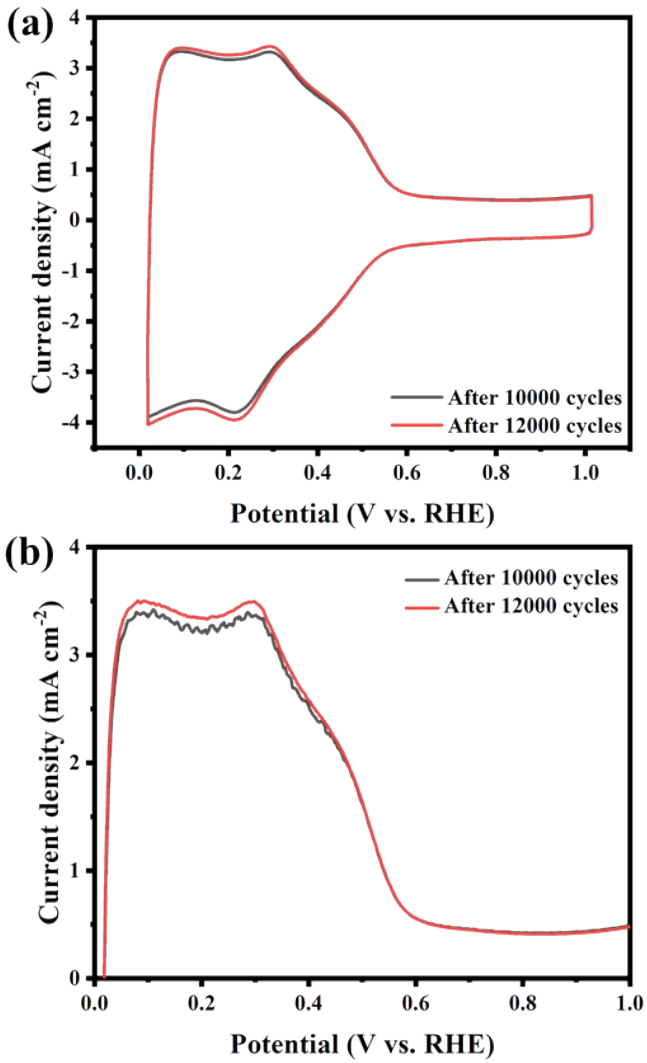

Figure S6. (a) CV curves of WC/WO_2 after 10000 and 12000 HOR cycles in H_2 saturated 0.5 M H_2SO_4 solution and the corresponding (b) LSV curves at the rotation speed of 1600 rpm.

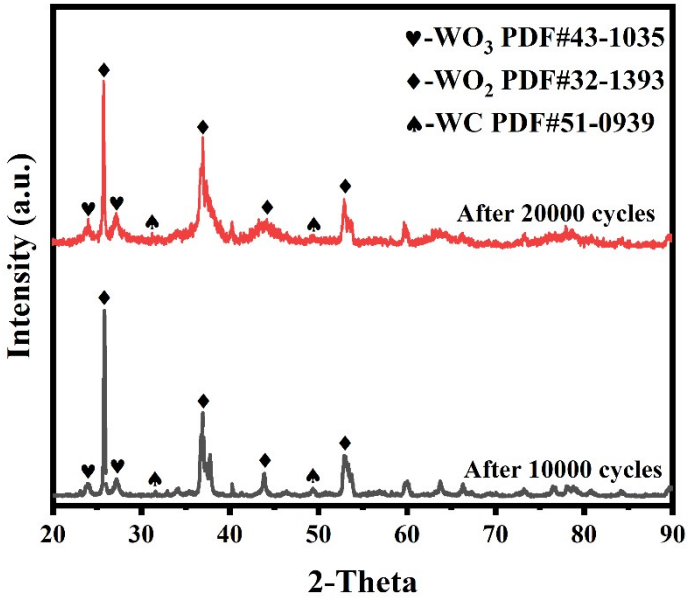

Figure S7. XRD patterns of pristine WC/WO_2 after 10000 and 20000 HOR cycles.

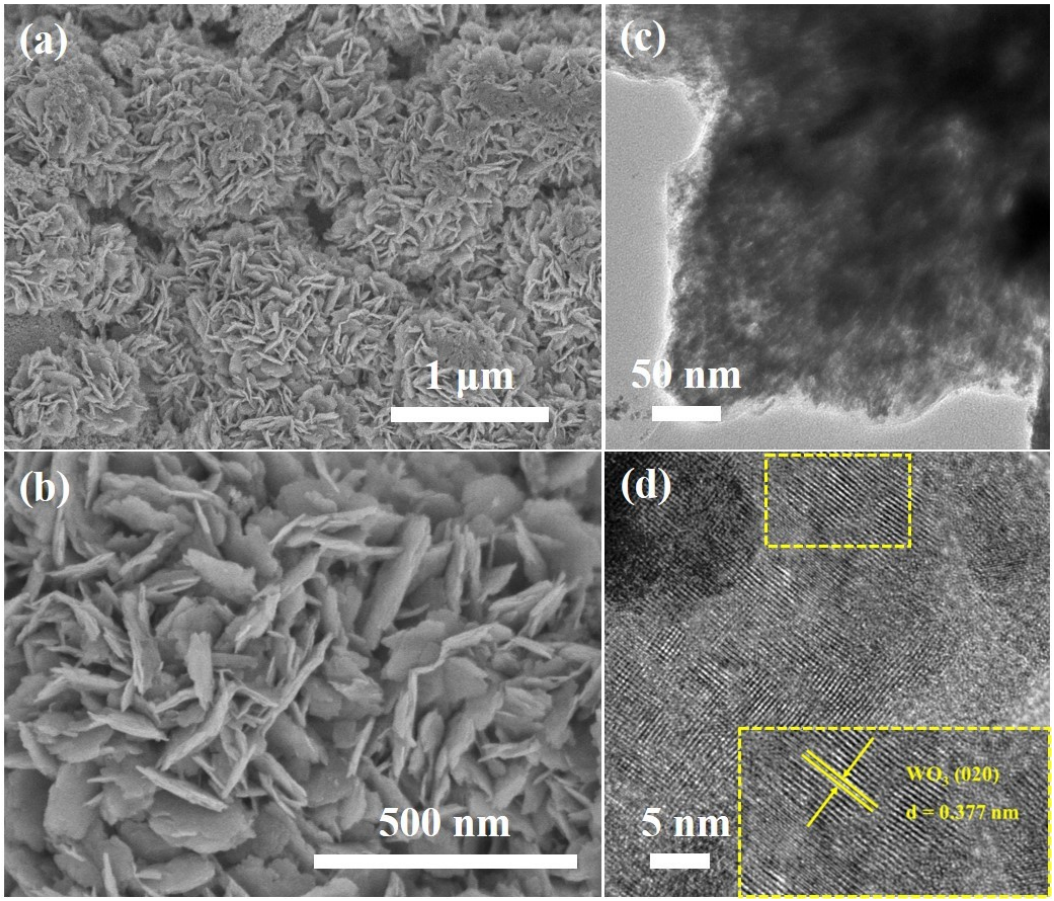

Figure S8. (a, b) SEM images, (c) TEM image and (d) HRTEM image of WC/WO_2 after 20000 HOR cycles.

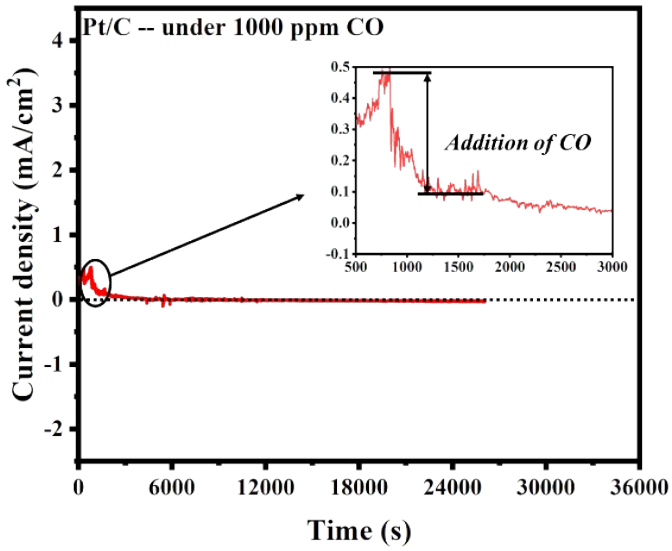

Figure S9. Stability tests of commercial Pt/C under the presence of 1000 ppm CO/H_2-saturated 0.5 M H_2SO_4 at the potential of 0.1 V (vs. RHE).

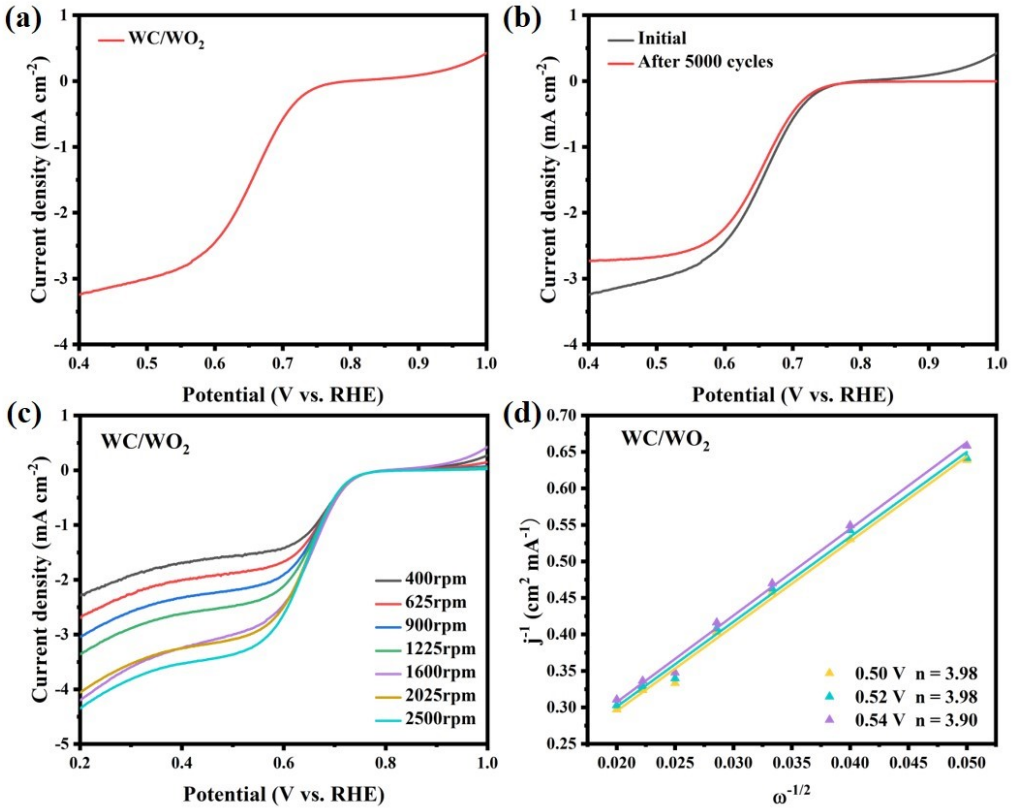

Figure S10. ORR performance of WC/WO_2 catalyst in O_2-saturated 0.1M KOH solution. (a) LSV polarization curves. (b) LSV polarization curves before and after 5000 ORR cycles at the rotation speed of 1600 rpm. (c) LSV polarization curves at different rotation rates with the scan rate of 5 mV/s. (d) K-L plot and the corresponding electron transfer numbers (n) at various potentials. (The LSV curves of oxygen reduction reaction (ORR) were measured in O_2-saturated 0.1M KOH solution at a scan rate of 5 mV/s at a rotating speeds of 400 - 2500 rpm.)

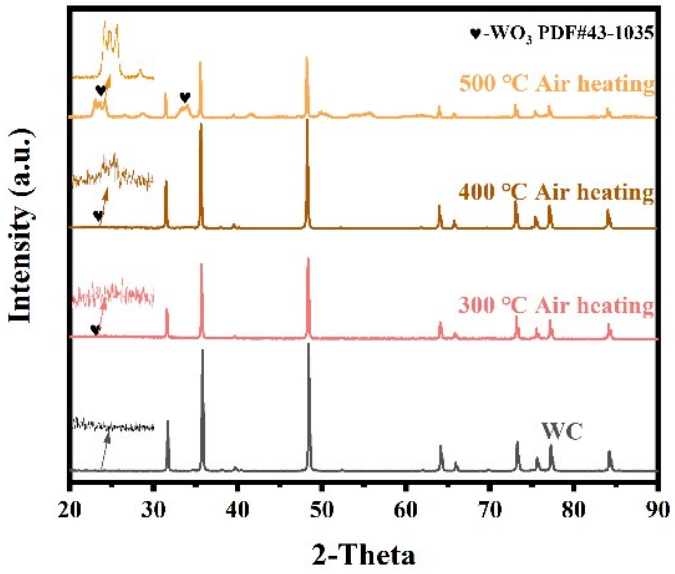

Figure S11. XRD patterns of WC and partial-oxidized WC at different heat treatment temperatures.

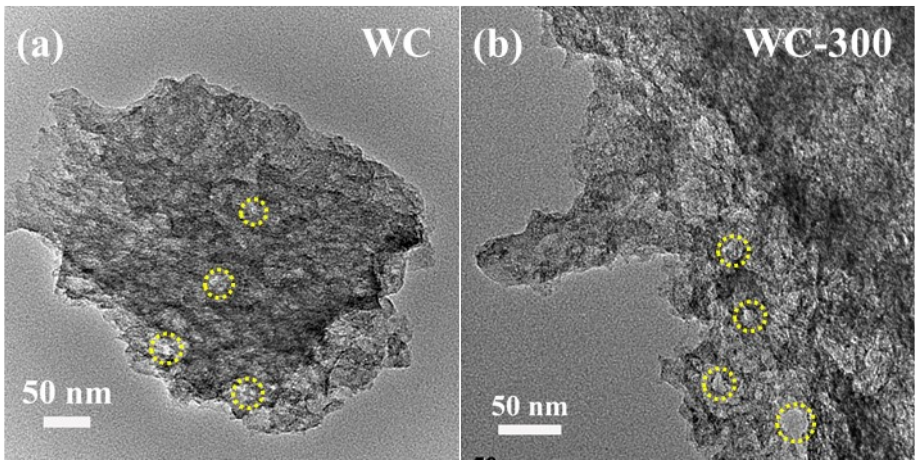

Figure S12. TEM images of WC (a) and WC-300 (b).

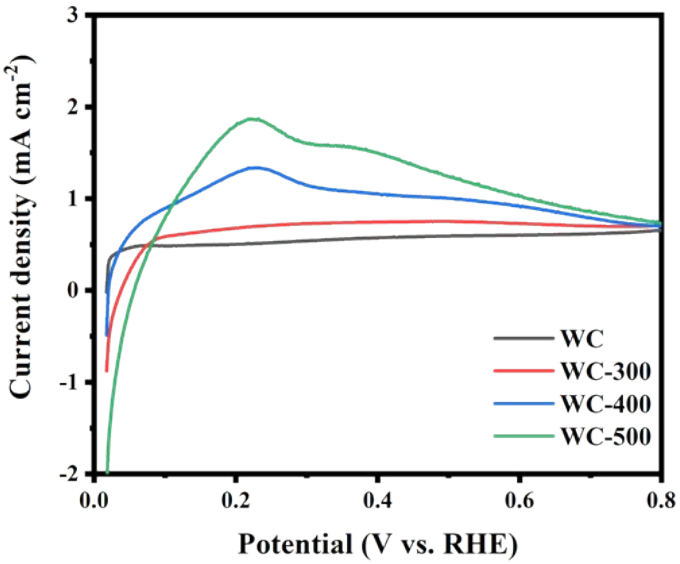

Figure S13. LSV curves of WC and partial-oxidized WC at the rotation speed of 1600 rpm.

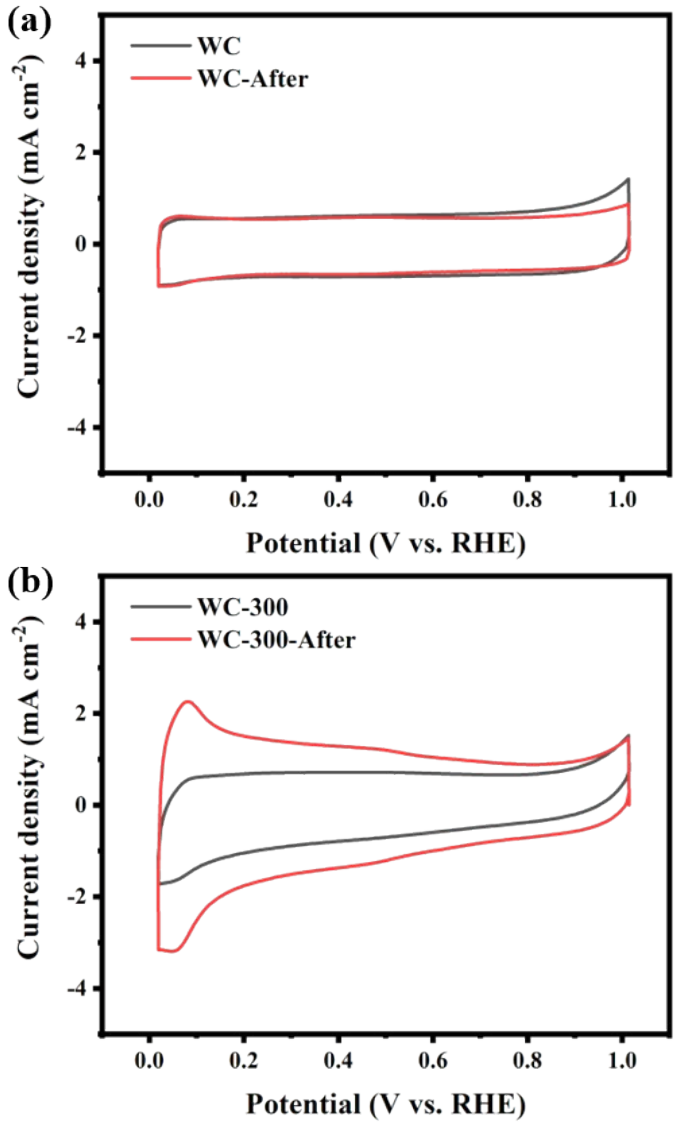

Figure S14. CV curves of WC (a) and WC-300 (b) before and after 10000 HOR cycles.

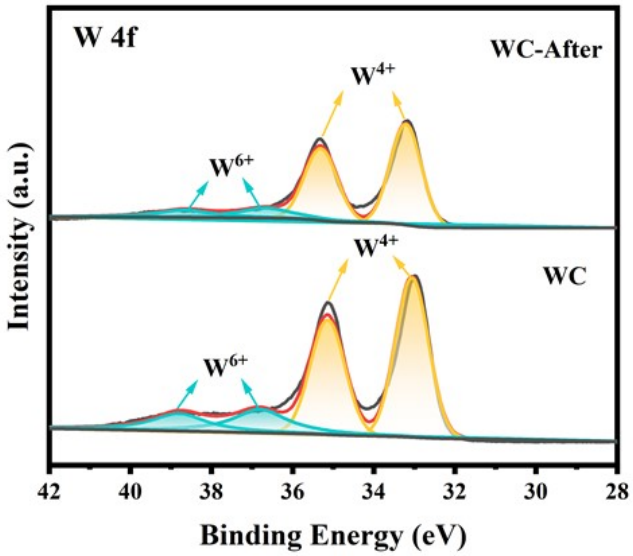

Figure S15. XPS W 4f spectra of WC before and after 10000 HOR cycles.

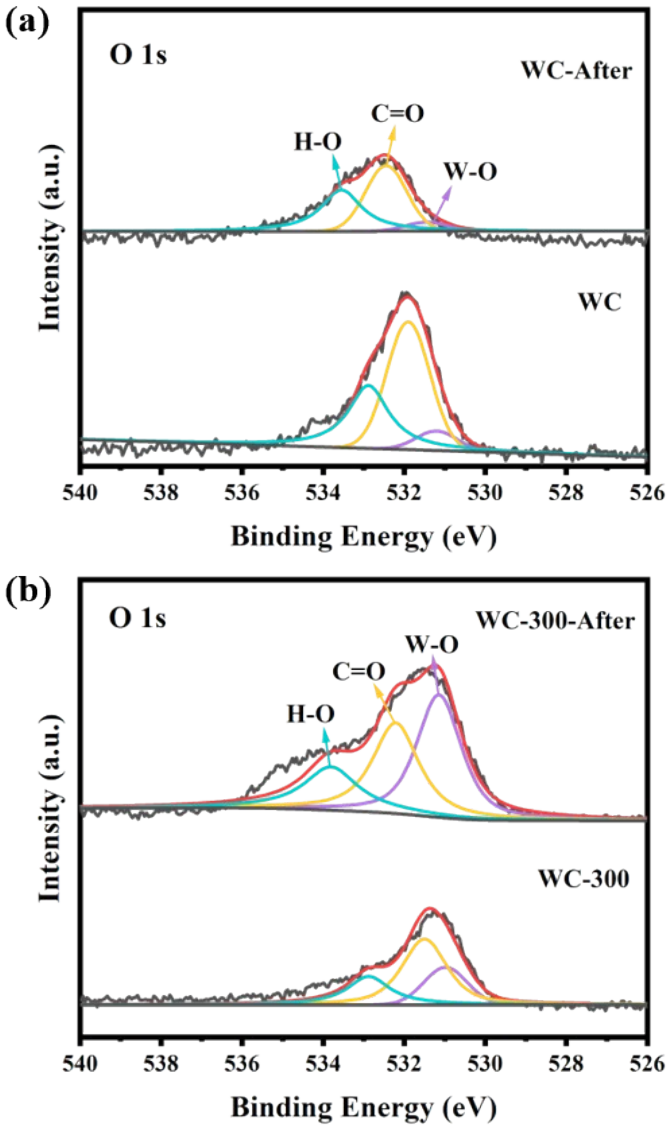

Figure S16. XPS O 1s spectra of WC (a) and WC-300 (b) before and after 10000 HOR cycles.

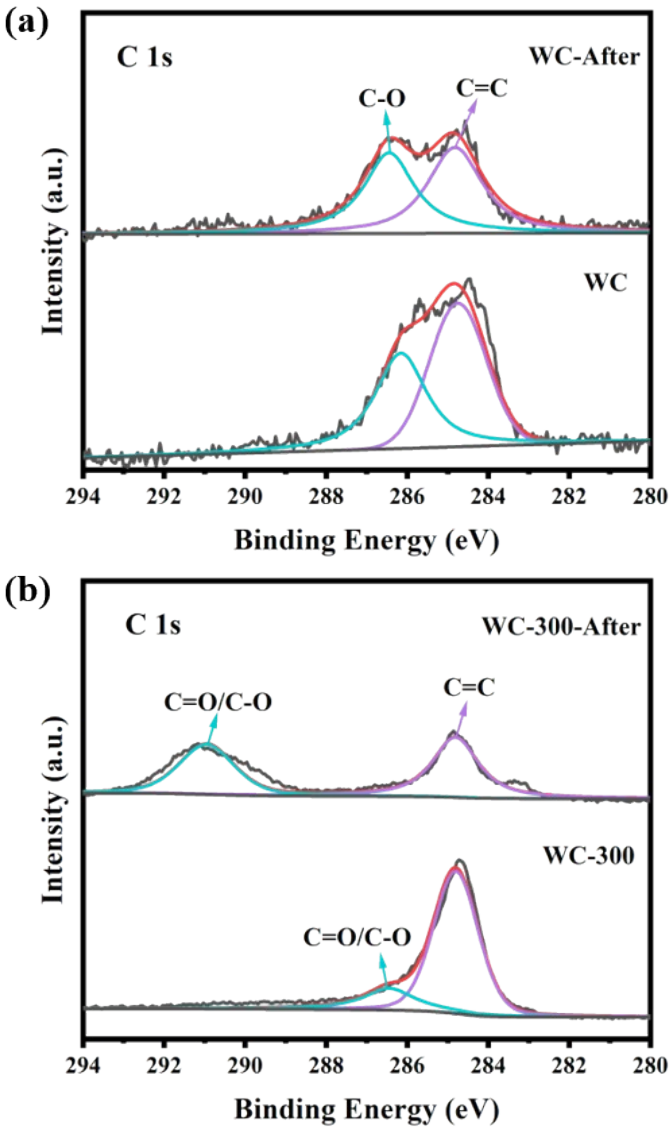

Figure S17. XPS C 1s spectra of WC (a) and WC-300 (b) before and after 10000 HOR cycles.

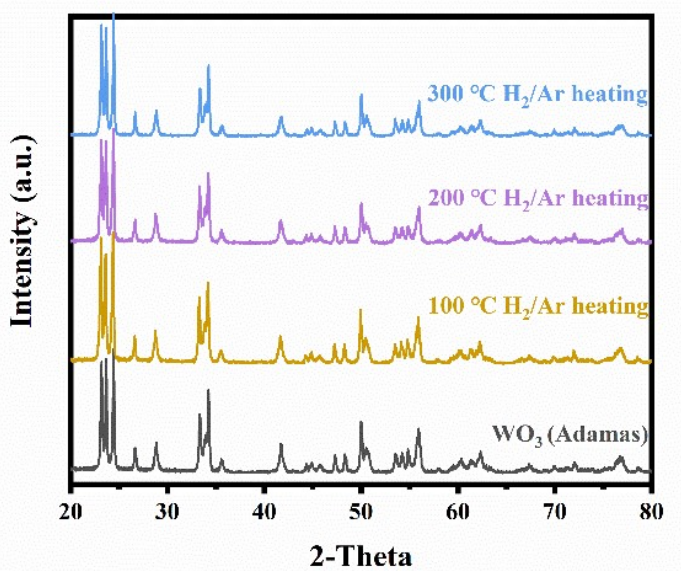

Figure S18. XRD patterns of WO_3 and partial-reduced WO_3 at different heat treatment temperatures.

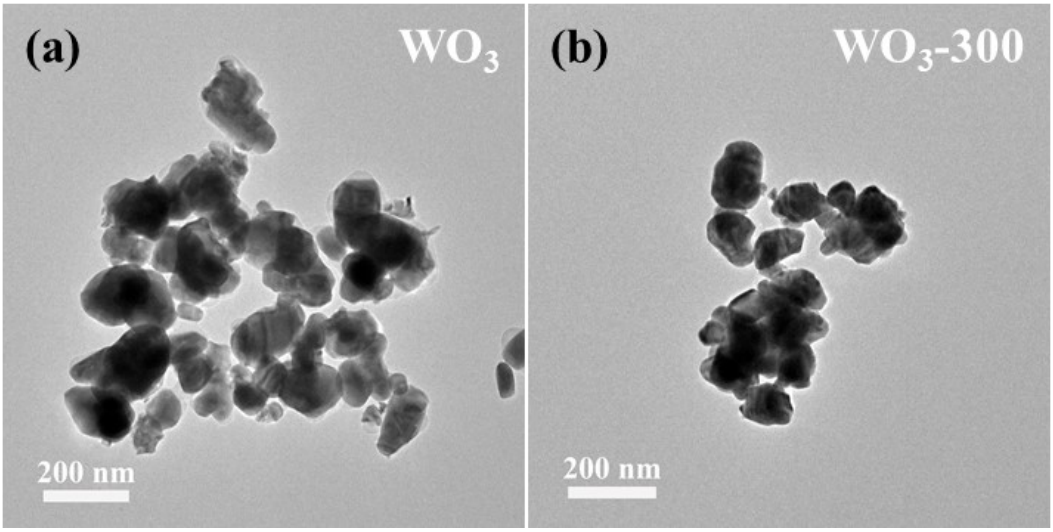

Figure S19. TEM images of WO_3 (a) and WO_3-300 (b).

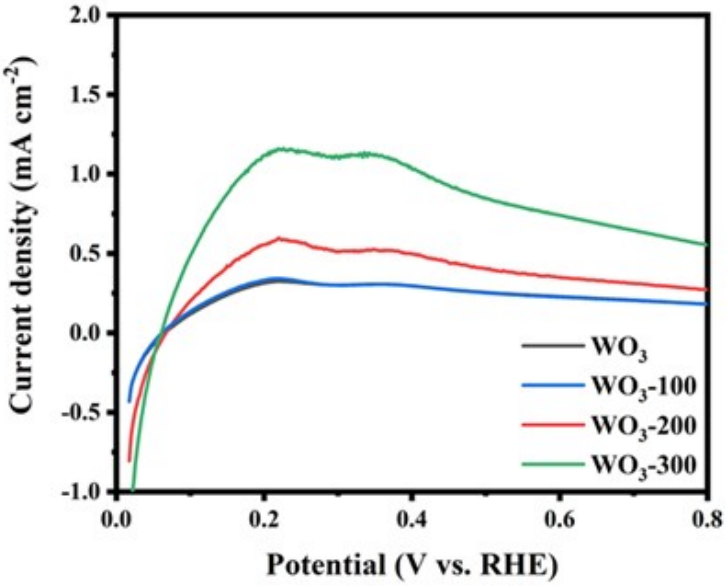

Figure S20. LSV curves of WO_3 and partial-reduced WO_3 at the rotation speed of 1600 rpm.

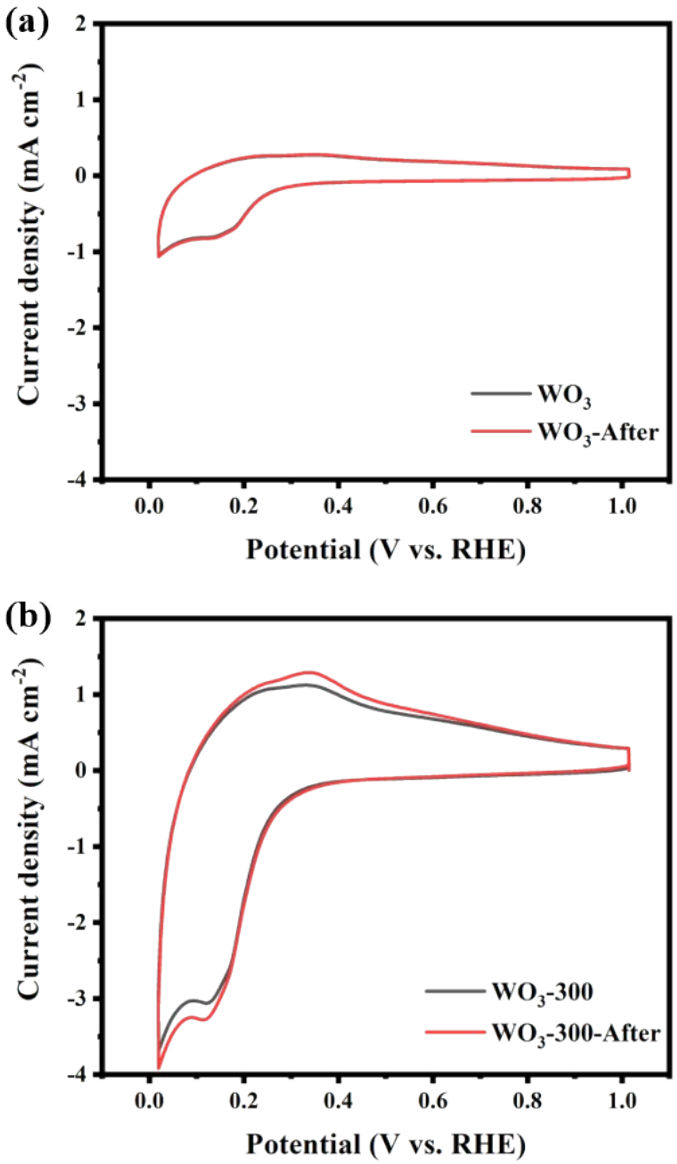

Figure S21. CV curves of WO_3 (a) and WO_3-300 (b) before and after 10000 HOR cycles.

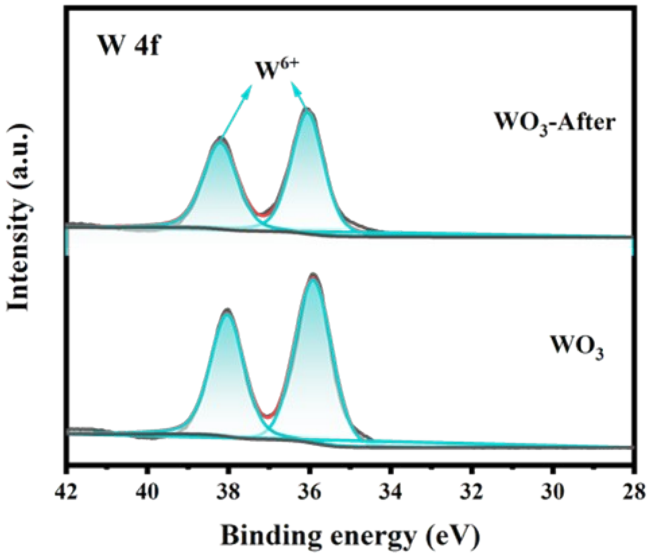

Figure S22. XPS W 4f spectra of WO_3 before and after 10000 HOR cycles.

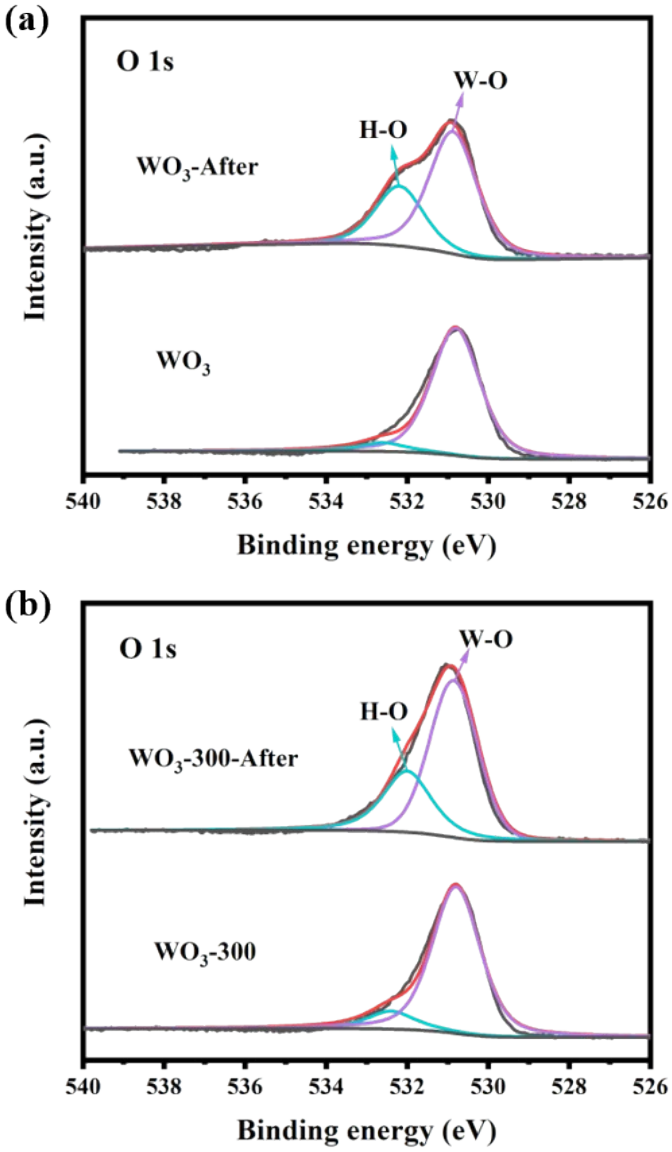

Figure S23. XPS O 1s spectra of WO_3 (a) and WO_3-300 (b) before and after 10000 HOR cycles.

Table S1. The ratio of W^{x+} (x=4/5/6) to total W from the XPS W 4f spectra of WC/WO_2, WC, WC-300, WO_3 and WO_3-300 before and after 10000 HOR cycles.

Catalyst	% Area of W^{4+}	% Area of W^{5+}	% Area of W^{6+}
WC/WO_2	53.5	6.7	39.8
WC/WO_2-After	29.2	-	70.8
WC	73.5	-	26.5
WC-After	79.3	-	20.7
WC-300	55.4	13.7	30.9
WC-300-After	63.8	-	36.2
WO_3	-	-	100
WO_3-After	-	-	100
WO_3-300	14.4	13.3	72.3
WO_3-300-After	8.4	9.9	81.7

Catalyst	HOR current density （mA/cm^2）	Fuel cell power density （mW/cm^2）	Paper
This work	~ 3.4	~ 200	-
W_2C@NPC	~ 1.8	-	Adv. Funct. Mat., 2019.[1]
IrNi/C	~ 2.6	-	Chin. J. Catal., 2016.[2]
Ru@TiO_2	~ 2.9	-	Nat. Catal., 2020.[3]
Pd/C	~ 3.0	-	J. Electrochem. Soc., 2016.[4]
1.5 Pd-$WO_{2.72}$-L	~ 5.2	-	Nano Res. 2021.[5]
PdO-RuO_2/C	~ 4.5	-	ChemSusChem, 2021.[6]
IrP_2-rGO	~ 2.5	-	ACS Appl. Mater. Interfaces, 2020.[7]
PdRu-WO_x/C	~ 3.1	-	Catal. Today, 2014.[8]
$Ni_xMo_{1-x}O_2$	~ 0.95	-	ACS Energy Lett., 2020.[9]
Pd-Co/gCN	-	~ 290	Appl. Energy, 2017.[10]

Table S2. HOR performances in acidic media in the latest reported literature.

Reference

(1) Xiong, B. Y.; Zhao, W. B.; Chen, L. S.; Shi, J. L., One-Step Synthesis of W_2C@N,P-C Nanocatalysts for Efficient Hydrogen Electrooxidation across the Whole pH Range. *Adv. Funct. Mater.* **2019**, *29*, 9.

(2) Liao, J. H.; Ding, W.; Tao, S. C.; Nie, Y.; Li, W.; Wu, G. P.; Chen, S. G.; Li, L.; Wei, Z. D., Carbon supported IrM (M = Fe, Ni, Co) alloy nanoparticles for the catalysis of hydrogen oxidation in acidic and alkaline medium. *Chem. Rev.* **2016**, *37*, 1142-1148.

(3) Zhou, Y. Y.; Xie, Z. Y.; Jiang, J. X.; Wang, J.; Song, X. Y.; He, Q.; Ding, W.; Wei, Z. D., Lattice-confined Ru clusters with high CO tolerance and activity for the hydrogen oxidation reaction. *Nat. Catal.* **2020**, *3*, 454-462.

(4) Zheng, J.; Zhou, S. Y.; Gu, S.; Xu, B. J.; Yan, Y. S., Size-Dependent Hydrogen Oxidation and Evolution Activities on Supported Palladium Nanoparticles in Acid and Base. *J. Electrochem. Soc.* **2016**, *163*, F499-F506.

(5) Peng, L.; Tian, H.; Cui, X.; Su, L.; Meng, G.; Ma, Z.; Cao, S.; Shi, J,. Dual synergetic catalytic effects boost hydrogen electric oxidation performance of Pd/$W_{18}O_{49}$. *Nano Res.* **2021**.

(6) Samanta, R.; Mishra, R.; Barman, S., Interface- and Surface-Engineered PdO-RuO_2 Hetero-Nanostructures with High Activity for Hydrogen Evolution/Oxidation Reactions. *Chemsuschem* **2021**, *14*, 2112-2125.

(7) Pu, Z.; Liu, T.; Zhao, W.; Shi, X.; Liu, Y.; Zhang, G.; Hu, W.; Sun, S.; Liao, S., Versatile Route To Fabricate Precious-Metal Phosphide Electrocatalyst for Acid-Stable Hydrogen Oxidation and Evolution Reactions. *ACS Appl. Mater. Interfaces* **2020**, *12*, 11737-11744.

(8) Kwon, K.; Jin, S. A.; Lee, K. H.; You, D. J.; Pak, C., Performance enhancement of Pd-based hydrogen oxidation catalysts using tungsten oxide. *Catal. Today* **2014**, *232*, 175-178.

(9) Zeng, H.; Chen, S.; Jin, Y. Q.; Li, J.; Song, J.; Le, Z.; Liang, G.; Zhang, H.; Xie, F.; Chen, J.; Jin, Y.; Chen, X.; Meng, H., Electron Density Modulation of Metallic MoO_2 by Ni Doping to Produce Excellent Hydrogen Evolution and Oxidation Activities in Acid. *ACS Energy Lett.* **2020**, *5*, 1908-1915.

(10) Ghosh, A.; Chandran, P.; Ramaprabhu, S. Palladium-nitrogen coordinated cobalt alloy towards hydrogen oxidation and oxygen reduction reactions with high catalytic activity in renewable energy generations of proton exchange membrane fuel cell. *Appl. Energy* **2017**, *208*, 37-48.